Inorganic Chemistry

Article

pubs.acs.org/IC

$Na_{2+x}Ti_6O_{13}$ as Potential Negative Electrode Material for Na-Ion Batteries

Kun Shen and Marnix Wagemaker*

Faculty of Applied Sciences, Delft University of Technology, Mekelweg 15, 2629JB, Delft, The Netherlands

Supporting Information

ABSTRACT: Na-ion batteries provide one of the most promising alternatives for Li-ion batteries due to the high abundance and low cost of Na. The strongly electropositive character of Na enables almost comparable cell potentials. Here we show that by lowering the cutoff voltage from 0.3 to 0 V vs Na/Na^+ the capacity of the $Na_2Ti_6O_{13}$ negative electrode material can be enhanced from 49.5 mAh/g ($Na_{2+1}Ti_6O_{13}$) to a promising 196 mAh/g ($Na_{2+4}Ti_6O_{13}$) for at least 10 cycles, after which it gradually reduces. To understand the structural changes in situ X-ray diffraction is performed and compared with density functional theory calculations. A consistent picture of the evolution in lattice parameters and Na-ion positions is presented. The results show that Na-ion intercalation in the $Na_{2+x}Ti_6O_{13}$ host structure is limited to $Na_{2+2}Ti_6O_{13}$ and proceeds through a solid solution reaction. Only small changes in lattice parameters promote that the insertion reaction is highly reversible. Further increasing the Na composition below 0.3 V appears to lead to loss in crystallinity, which in combination with solid electrolyte interface formation is suggested to be the origin of the gradually reducing reversible capacity.

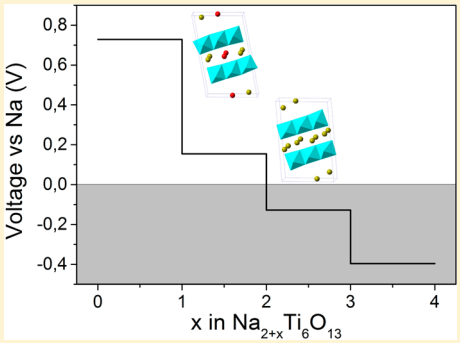

INTRODUCTION

The demand for renewable energy resources has initiated the search for high performance and cost-effective battery systems. Li-ion batteries have the highest energy densities, making them in particular suitable for mobile devices. However, considering applications where energy density is less important, for instance in static storage devices, the high cost of Li-ion batteries is an important concern. This has resulted in a growing interest in other battery systems such as Na-ion batteries. The Na-ion battery is one of the most promising alternatives due to its high abundance, low cost, and high cell potential. In the past decades, research on Na-ion batteries has been initiated in parallel with Li-ion battery research,[1−6] however the success of the latter has largely diverted attention away from Na-ion batteries. Renewed interest in Na-ion batteries is motivated by the virtually unlimited Na resources and low costs.[7,8] In general, the operating voltage of Na-ion batteries is about 0.4 V lower compared to Li-ion batteries, resulting in a somewhat lower but still large energy and power density.[9] Compared with Li ions (0.76 Å), the larger ionic radius of Na ions (1.02 Å) often leads to larger structural distortions and barriers for diffusion in host structures.[9] This is most likely the reason why only a few insertion electrode materials are reported displaying reversible Na-ion uptake, negative electrode materials being in particular scarce. Sodium metal as a negative electrode introduces complications such as dendrite formation, low melting point, and interface aging.[8] Graphite and hard carbons, extensively investigated as negative electrodes, have much lower specific capacities and result in larger capacity fading compared to application in Li-ion batteries.[10−12] In addition, the capacitive storage of Na-ions at the graphite surface has the disadvantage of a linear drop in the battery voltage lowering the energy density.[13] Due to the competition between inversion and conversion reactions, only the 3d metal (Ti,V) oxides appear promising for low voltage Na-ion insertion.[14] Na_xVO_2 was found to react reversibly around 1.5 V.[15,16] At the same potential, amorphous TiO_2 nanotubes and nanocrystalline TiO_2 anatase demonstrated a specific capacity of ∼150 mAh/g.[17−20] A reversible storage capacity of 200 mAh/g was achieved in $Na_2Ti_3O_7$ applying a cutoff voltage of 0 V vs Na/Na^+.[21] Recently, Rudola et al. explored Na-ion storage in the structurally similar $Na_2Ti_6O_{13}$ compound, demonstrating a reversible uptake of 1 Na ion per formula unit (49.5 mAh/g) by a solid solution mechanism at an average potential of 0.8 V when $Na_2Ti_6O_{13}$ vs Na/Na^+ is cycled between 2.5 and 0.5 V.[22]

Motivated by the higher storage capacities of the similar $Na_2Ti_3O_7$ material, the present study explores Na-ion storage in $Na_2Ti_6O_{13}$ at low voltages. In situ and ex situ X-ray diffraction in combination with density functional theory (DFT) calculations reveal the intercalation mechanism, giving a consistent picture of the structural changes and electrochemical performance of this promising Na-ion negative electrode.

EXPERIMENTAL SECTION

Materials Synthesis. $Na_2Ti_6O_{13}$ was prepared by ball milling Na_2CO_3 (Aldrich) and TiO_2 anatase (Aldrich) in a mass ratio of 0.22:1 in a silicon carbide crucible applying a 250 rpm rate for 120 min.

Received: February 23, 2014
Published: July 31, 2014

   dx.doi.org/10.1021/ic5004269 | Inorg. Chem. 2014, 53, 8250−8256

Subsequently, this precursor mixture was heated at 800 °C in open air for 12 h, applying a heating and cooling ramp rate of 5 °C/min. X-ray diffraction analysis confirmed the crystalline $Na_2Ti_6O_{13}$ phase indexed with the monoclinic $C2/m$ space group and a crystallite size of approximately 80 nm. Additionally a small amount of approximately 5% of unreacted TiO_2 anatase and trace amounts (less than 1%) of $Na_2Ti_3O_7$ and Na_2CO_3 were identified, the latter explaining the presence of unreacted TiO_2.

Electrode Preparation. For the electrochemical tests and ex situ X-ray diffraction measurements electrodes were prepared by mixing the active $Na_2Ti_6O_{13}$ material with the polyvinylidene fluoride (PVDF) binder (Aldrich) and carbon black (ENSAQO) in the weight ratio 8:1:1 using *N*-methyl-2-pyrrolidone (NMP) (Aldrich) as solvent. The well-mixed slurry was coated on carbon coated aluminum foil by doctor blading followed by 100 °C overnight drying.

For the in situ X-ray diffraction measurements self-supporting electrode films were prepared. PVDF (0.42g) and DBP (dibutyl phthalate) (0.34 g) were dissolved in acetone. The active material $Na_2Ti_6O_{13}$ (0.7 g) and conductive additive carbon black (ENSAQO) (0.28 g) were well mixed and added in the PVDF and DBP solution. The slurry was cast on glass by doctor blading. After drying the electrode film was washed with diethyl ether in order to dissolve DBP. Finally the coatings were dried at 100 °C overnight.

Electrochemistry. Electrochemical tests were carried out in Swagelok type electrochemical cells. The $Na_2Ti_6O_{13}$ electrodes were (dis)charged versus sodium metal with 1 M $NaClO_4$ in propylene carbonate serving as electrolyte and a cotton microfiber separator (Whatman). The cells were assembled in a glovebox under argon atmosphere (O_2 < 0.1 ppm and H_2O < 0.1 ppm). The (dis)charge cycling tests were performed at $C/10$ rate (4 mA/g) at room temperature with a MACCOR S4000 cycler.

X-ray Diffraction. In situ and ex situ X-ray diffraction was performed using a Panalytical X'pert Pro X-ray diffractometer employing Cu Kα radiation in the range 10−130° and 10−100°, respectively. For the ex situ X-ray diffraction characterization, the $Na_2Ti_6O_{13}$ vs Na/Na^+ cell was discharged to 0 V and the positive electrode was removed from the cell and assembled in a Kapton covered airtight X-ray diffraction sample holder. All these operations were performed in a glovebox under argon atmosphere (O_2 < 0.1 ppm and H_2O < 0.1 ppm).

In situ X-ray diffraction was performed in a home designed airtight electrochemical cell with a beryllium window acting as current collector largely transparent for X-rays. The airtight electrochemical cell was assembled in a glovebox under argon atmosphere (O_2 < 0.1 ppm and H_2O < 0.1 ppm) with sodium metal as negative electrode, cotton microfiber as separator (Whatman), and 1 M $NaClO_4$ in propylene carbonate serving as electrolyte. A thin aluminum foil (2 μm) was used to restrict X-ray absorption losses and to separate the $Na_2Ti_6O_{13}$ electrode from the beryllium foil window to avoid potential corrosion of the beryllium. In situ XRD data was restricted to a cutoff voltage of 0.3 V because cycling to ∼0 V in the in situ cell leads, even of the presence of the 2 μm Al foil, to corrosion of the Be and potential leaking of the cell. For this reason ex situ XRD experiments were performed below 0.3 V. Compared to conventional electrodes, this special in situ configuration leads to no significant changes in the voltage and capacity at the low currents applied, indicating that the diffraction data collected from this in situ cell represents the electrochemistry of the conventional electrodes. For in situ measurement diffraction patterns were collected during the galvanostatic (dis)charge using a MACCOR S4000 cycler. For the $C/10$ (dis)charge rate a collection time of 1 h was used to obtain reasonable time resolution following the structural evolution at the $C/10$ rate in combination with patterns having enough statistics to be refined. The consequence is that each pattern represents an average of the structural evolution during 1 h. The X-ray diffraction patterns were refined using the Rietveld refinement method as implemented in GSAS.[23]

DFT Calculations. The $Na_{2+x}Ti_6O_{13}$ structures were geometrically optimized by applying the gradient-corrected exchange correlation functional (GGA) to density functional theory calculations as implemented in the plane wave code VASP.[24−26] Spin-polarization was not considered. All structures were fully relaxed to the ground state. A cutoff energy of 400 eV and appropriate *k*-point grid was chosen to ensure that total energies converged within 10^{-4} eV per formula unit. DFT molecular dynamics simulations were performed on $Na_{2+4}Ti_6O_{13}$ unit cell for 3 ps with time step of 2 fs at two temperatures (300 and 400 K).

RESULTS AND DISCUSSION

Electrochemistry. Figures 1a and 1b illustrate the impact of the cutoff voltage on the voltage-capacity profile of $Na_2Ti_6O_{13}$

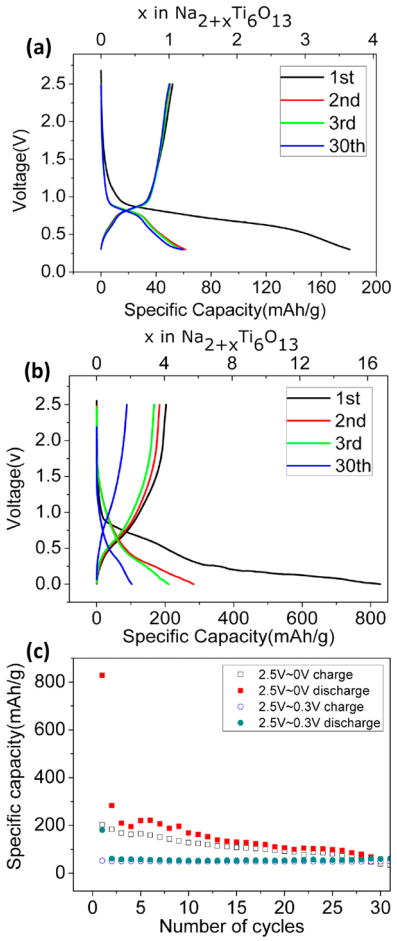

Figure 1. Electrochemical characterization of $Na_2Ti_6O_{13}$ vs Na/Na^+. (a) First three cycles and the 30th cycle of the galvanostatic (dis)charging of $Na_2Ti_6O_{13}$ at $C/10$ rate (0.005 A/g) down to 0.3 V vs Na/Na^+. (b) First three cycles and the 30th cycle of the galvanostatic (dis)charging of $Na_2Ti_6O_{13}$ at $C/10$ rate (0.005 A/g) down to 0.0 V vs Na/Na^+. (c) Specific capacity as a function of the number of cycles at $C/10$ rate.

versus sodium metal at $C/10$ rate ($1C$ is defined as the current required to fully discharge/charge the $Na_2Ti_6O_{13}$ electrode in 1 h assuming the maximum composition is $Na_3Ti_6O_{13}$). Upon reducing the cutoff voltage from 0.3 to 0 V, three distinct changes are observed: (i) When a cutoff voltage of 0.3 V is applied, a reversible voltage plateau-like feature appears around 0.8 V. This is replaced by a more gradual voltage decrease when the cutoff voltage is set to 0 V. (ii) Both the first discharge capacity and the initial reversible capacity at a cutoff voltage of 0 V are four times larger compared to that at 0.3 V cutoff voltage. To rule out the contribution of carbon black and

dx.doi.org/10.1021/ic5004269 | Inorg. Chem. 2014, 53, 8250−8256

PVDF additive to the capacity, blank cells containing only carbon black and PVDF were prepared. Comparison with the galvanostatic tests of the blank cells demonstrates that, for the first discharge, carbon and PVDF contribute in total 75% to the capacity for both cutoff voltages, which is mainly irreversible as it contributes less than 10% to the reversible capacity for the subsequent cycles (see the Supporting Information). Therefore, based on the electrochemical measurements, we conclude that galvanostatic cycling between 2.5 and 0.3 V leads to the reversible intercalation of one additional sodium ion in the structure ($Na_3Ti_6O_{13}$), while galvanostatic cycling between 2.5 and 0 V leads to the reversible reaction of four additional sodium ions in the structure ($Na_6Ti_6O_{13}$). (iii) Figure 1c shows that cycling between 2.5 and 0.3 V leads to excellent capacity retention after 30 cycles amounting to more than 95% of the initial charge capacity (disregarding the first cycle). By lowering the cutoff voltage to 0 V the capacity is larger but the reversible capacity retention drops to approximately 75% over 30 cycles. To reveal the origin of the larger capacity and poor capacity retention when the material is cycled down to 0 V cutoff voltage, in situ, ex situ diffraction and DFT calculations were performed.

X-ray Diffraction. In situ X-ray diffraction measurements have been performed to investigate the structural changes of the $Na_2Ti_6O_{13}$ electrode material upon cycling between 2.5 and 0.3 V. In addition ex situ XRD patterns were collected at 2.5, 0.3, and 0 V to reveal the structural changes in the low potential region (0 V cutoff). Excellent reversibility of the structural changes above 0.3 V is confirmed by the reversible evolution of the Bragg peaks recorded during the charge, shown in Figure 2.

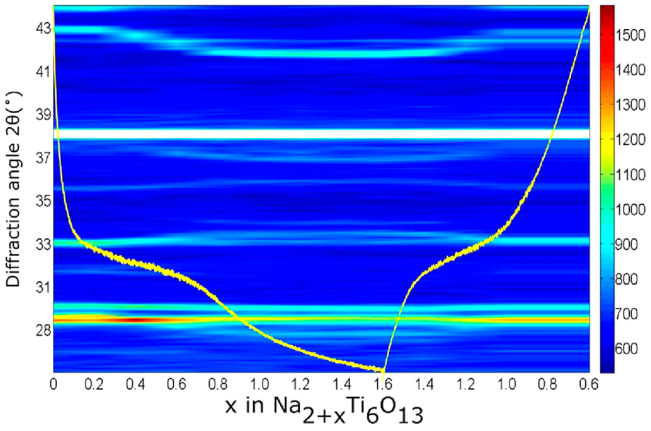

Figure 2. Evolution of in situ X-ray diffraction patterns as a function of Na composition. The yellow line represents the voltage profile down to 0.3 V, as a function of intercalated Na composition. The sodium composition x in $Na_{2+x}Ti_6O_{13}$ is estimated by the capacity measured by the galvanostatic electrochemistry.

The irreversible capacity observed during the in situ diffraction measurement in Figure 2 is due to the first cycle irreversible capacity loss of the carbon and PVDF present in the electrodes discussed above.

X-ray diffraction of the prepared $Na_2Ti_6O_{13}$ material confirms the monoclinic $C2/m$ space group having a 3D tunnel structure in which the initially present Na ions reside, as shown in Figure 3. The lattice parameters of the structure are a = 15.10 Å, b = 3.75 Å, c = 9.16 Å, and β = 99.15° consistent with previous studies.[27−29] In situ X-ray diffraction patterns collected at various sodium compositions between x = 0 and x = 1 in $Na_{2+x}Ti_6O_{13}$ are shown in Figure 4a. The continuous shift of the original $Na_2Ti_6O_{13}$ {60−1} and {40−4} reflections indicates a gradual change in lattice parameters, which is consistent with the structural study on sodium intercalation into $Na_2Ti_6O_{13}$.[22] The {020} reflection splits into two reflections indexed as {020} and {80$\bar{1}$} where the {020} reflection intensity weakens. The same phenomenon is observed for the {402} reflection at lower angle. Remaining

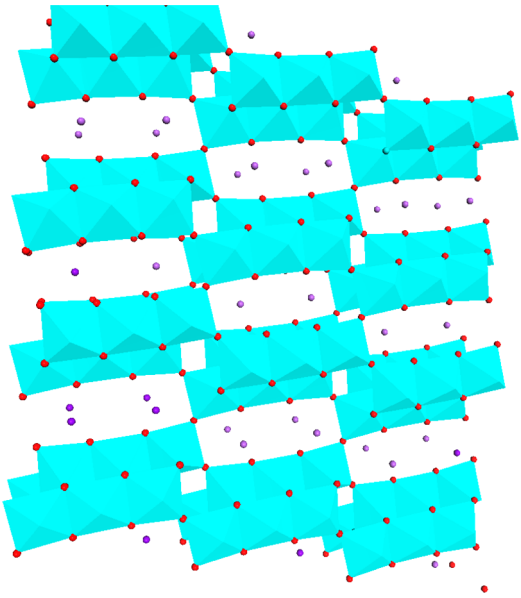

Figure 3. Monoclinic crystal structure of $Na_2Ti_6O_{13}$ displaying the tunnels in which the Na ions reside. Purple spheres represent sodium ions, red spheres represent oxygen, and cyan polyhedrons represent the Ti−O octahedra.

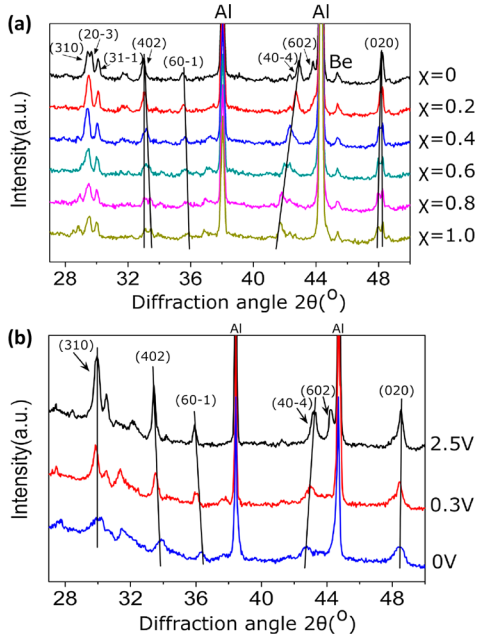

Figure 4. (a) Evolution of in situ X-ray diffraction patterns of the $Na_{2+x}Ti_6O_{13}$ (x indicating the additional Na composition) electrode during the second discharge between 2.5 and 0.3 V. (b) Ex situ X-ray diffraction patterns at 2.5, 0.3, and 0 V for the $Na_{2+x}Ti_6O_{13}$ cycling between 2.5 and 0 V.

dx.doi.org/10.1021/ic5004269 | Inorg. Chem. 2014, 53, 8250−8256

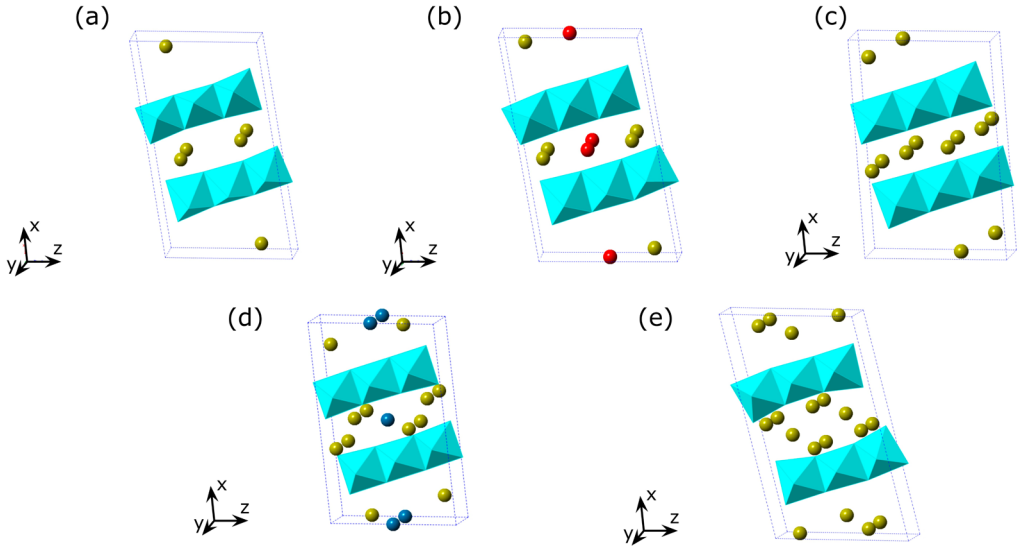

Figure 5. DFT predicted monoclinic crystal structures of $Na_{2+x}Ti_6O_{13}$. (a) $Na_2Ti_6O_{13}$, (b) $Na_{2+1}Ti_6O_{13}$, (c) $Na_{2+2}Ti_6O_{13}$, (d) $Na_{2+3}Ti_6O_{13}$, (e) $Na_{2+4}Ti_6O_{13}$. Yellow spheres represent sodium ion 4i sites, red spheres represent sodium 2d sites, dark blue spheres represent sodium 2c sites, and cyan polyhedrons represent the Ti−O octahedra.

in the same space group, this is the consequence of the significant increase of the c lattice parameter and β.

Electrochemical discharging from 0.3 to 0 V indicates that three additional sodium ions may be intercalated per unit formula reaching the $Na_6Ti_6O_{13}$ composition. Comparing the ex situ XRD results at 0.3 and 0 V reveals that the main Bragg reflections {310}, {402}, {60$\bar{1}$}, {40$\bar{4}$} of $Na_2Ti_6O_{13}$ continue shifting (see Figure 4b) demonstrating that also in the low potential region (0.3−0 V) a solid solution reaction leads to gradual unit cell expansion. Even at 0 V the structure can still be indexed with the same monoclinic space group as the pristine $Na_2Ti_6O_{13}$ phase. In addition, it is observed that the reflections decrease in intensity and increase in width. This may indicate that the crystallinity and/or crystallite size of $Na_2Ti_6O_{13}$ reduces significantly upon Na-ion addition below 0.3 V.

DFT

X-ray diffraction reveals a solid solution reaction, however, not the Na-ion positions and occupancy in the $Na_{2+x}Ti_6O_{13}$ structure. Density functional theory calculations were used to predict the structure and average voltage of reduced phases at various compositions.

By evaluating the ground state energy of all possible sodium configurations in the $Na_{2+x}Ti_6O_{13}$ unit cell at every composition (x = 0, 1, 2, 3, and 4), insight can be gained in the structural evolution. Potential Na-ion sites were identified using DFT molecular dynamics simulations and Fourier density difference maps from the diffraction. Using DFT all potential positions were relaxed to the ground state and subsequently the total energies were calculated. The configuration with the lowest energy at each concentration is expected to occur upon actual Na intercalation, thereby only considering the configurational degree of freedom associated with Na-vacancy configurations in a single unit cell and neglecting the entropy contribution from lattice vibrations and electronic excitations. The DFT determined structures are shown in Figure 5, the structural details of which are listed in Table S.I.1 in the Supporting Information.

Compared to $Na_2Ti_6O_{13}$, the lowest energy configuration of $Na_{2+1}Ti_6O_{13}$, shown in Figure 5b, has very small changes in the Ti−O structure. The inserting Na ions are located on the 2d sites in the middle of the tunnel next to the already present Na ions occupying the 4i sites. This position leads to a smaller nearest Na−Na distance (decreasing from 3.745 to 2.878 Å). This sodium insertion of the tunnels also shortens the nearest Na−O distance from 2.632 to 2.469 Å. Increasing the composition from $Na_{2+1}Ti_6O_{13}$ to $Na_{2+2}Ti_6O_{13}$ is realized by migration of the Na ions from the 2d sites to adjacent 4i sites in the same plane as the already occupied 4i positions, further decreasing the nearest Na−Na distance to 2.482 Å and nearest Na−O distances to 2.241 Å. Upon further sodium intercalation, exceeding $Na_{2+2}Ti_6O_{13}$, the original intercalated sodium ions migrate from close to the center of the tunnels toward the edge of the Ti−O tunnel, forming half "Na−O octahedral" units, and the new Na ions insert into 2c sites located in the center of the tunnel as shown in Figures 5d and 5e. The nearest Na−O distance continuously decreases as the Na composition increases, from 2.149 to 2.130 Å, and as a consequence, the original nearest Na−Na distance is increased 2.607 Å in $Na_{2+3}Ti_6O_{13}$ to 2.649 Å in $Na_{2+4}Ti_6O_{13}$, indicating that the Na−Na distance is becoming too small leading to increasing repulsive Coulomb forces. The evolution of the lattice parameters suggests a variation of the shape of the 3D Ti−O tunnel upon Na insertion, resulting from the competition between the attractive Coulomb force (between the Na ions and oxygen forming the tunnels) and the repulsive Coulomb force (between the inserted Na ions).

A bond valence sum (BVS) analysis[30] was performed to evaluate the structural stability of the predicted Na inserted structures. The BVS value is estimated by $V = \sum V_i$, and the individual bond valences v_i are calculated from the observed bond lengths R_i by $v_i = \exp[(R_0 - R_i)/b]$ where R_0 = 1.803 and b = 0.37 were used for the Na−O bond,[30] the results of which are added to Table S.I.1 in the Supporting Information. If the BVS value of the insertion site is significantly larger than the formal valence of the Na ion, this indicates that the Na ion is too large to fit the interstitial site. For the reported $Na_2Ti_6O_{13}$ structure[22] the BVS value of the established Na position results in 0.37, relatively small compared to the expected value of 1. This may indicate that realistic Na-ion positions may result in

dx.doi.org/10.1021/ic5004269 | Inorg. Chem. 2014, 53, 8250−8256

relatively low BVS values in these compounds. For compositions $x = 1$ and $x = 2$ similar BVS values are found for the Na-ion positions (see the Supporting Information). For compositions $x = 3$ and $x = 4$ BVS values closer to 1 are obtained for the Na-ion positions and only one Na ion, the 2c site in $x = 3$, results in a significantly larger BVS value (+1.52) compared to the formal valence (+1) of the Na ion. This indicates that the $x = 3$ structure is unlikely to be formed, consistent with the conclusion below based on the DFT predicted voltages.

For comparison with the experimental electrochemical results, the intercalation voltages at different Na compositions are estimated based on the ground state energy of the most stable configurations according to

$$V(x) = -\frac{E_{Na_{2+x}Ti_6O_{13}} - E_{Na_2Ti_6O_{13}} - xE_{Na}}{xe} \quad (1)$$

The calculated average voltages in Figure 6 show that, as expected, increasing the Na composition lowers the voltage (in this case referenced to Na metal Na/Na^+) which is correlated to the evolution of the Na−O distance. The calculated average intercalation voltage of 0.728 V between $x = 0$ and $x = 1$ in $Na_{2+x}Ti_6O_{13}$ is in good agreement with the experimentally observed reversible voltage of approximately 0.8 V for these compositions, see Figure 1a. The underestimation of the potential by GGA is typical for transition metal oxides and the result of the self-interaction in the d-orbitals.[32] The predicted average voltage between the $x = 1$ and $x = 2$ compositions is approximately 0.15 V, indicating that these compositions are not formed above 0.3 V, consistent with the observations in Figure 1a. The DFT results in Figure 6 predict that the maximum composition that can be achieved at 0 V vs Na/Na^+ is $Na_{2+2}Ti_6O_{13}$. Increasing the composition from $x = 3$ to 4 results in negative voltages, implying that these compositions will not be formed in practice and that $Na_{2+2}Ti_6O_{13}$ is the upper limit for sodium insertion in bulk $Na_{2+x}Ti_6O_{13}$. However, electrochemical cycling down to 0 V after the first cycle, shown in Figure 1b, suggests a reversible composition up to $x = 4$ (~200 mAh/g), albeit degrading over several cycles, see Figure 1c. This capacity is not due to carbon and PVDF because this does contribute significantly to the total capacity after the first cycle (see Figure S.I.1 in the Supporting Information). The $x = 4$ composition is in contradiction with the DFT calculations that predict the maximum composition (leading to positive voltages vs Na/Na^+) of $x = 2$. Apparently, at these low voltages a different storage mechanism sets in as discussed below.

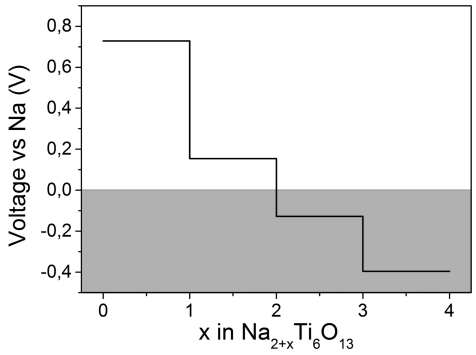

Figure 6. Calculated insertion voltage profile based on the DFT ground state energies as a function of the sodium composition.

Using the most stable $Na_{2+1}Ti_6O_{13}$ configuration from DFT as input for the Rietveld refinement of the XRD pattern results in a good fit, shown in Figure 7, implying minimal changes in the atomic positions and lattice parameters indicating that DFT predicts the structure accurately. The unit cell dimensions of $Na_{2+1}Ti_6O_{13}$ determined from the Rietveld refinement are shown in Table 1, and the atomic positions are given in Table S.I.1 in the Supporting Information. The small volume expansion (1%) between the original $Na_2Ti_6O_{13}$ and the $Na_{2+1}Ti_6O_{13}$ compositions suggests that mechanical failure of the material will not play a significant role, which is consistent with the excellent cycling stability observed above 0.3 V in Figure 1.

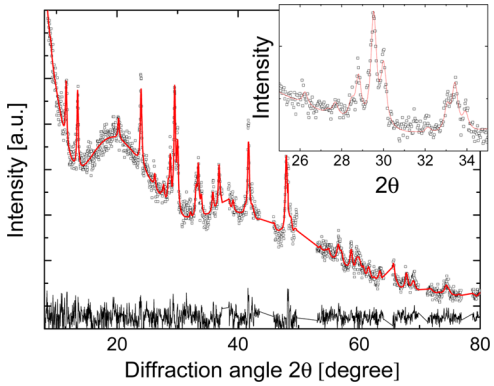

Figure 7. Rietveld refinement of the in situ X-ray diffraction pattern of $Na_{2+1}Ti_6O_{13}$ after the second discharge. Black symbols represent the experimental data, the solid line represents the Rietveld refinement, and at the bottom the difference between observed and calculated intensities is shown. The refined parameters include lattice parameters, atomic positions, a broadening parameter, and the temperature factor. The peaks from aluminum and beryllium have been excluded. The average agreement index parameters are $R_p = 4.0\%$ and $R_{wp} = 5.3\%$.

Table 1. Lattice Parameters of $Na_{2+x}Ti_6O_{13}$ Collected at Various Sodium Compositions[a]

	a	b	c	β	cell vol	x in $Na_{2+x}Ti_6O_{13}$
original	15.11	3.746	9.175	99.037	512.74	0
sample A at $x = 1$	14.88	3.757	9.415	100.587	517.35	1
sample B at 0 V	15.00	3.778	9.364	100.056	522.51	2.11

[a]The composition for sample A is estimated by the capacity resulting from the electrochemistry in Figure 1, and the composition of sample B is estimated assuming Vegard's law between $x = 0$ and $x = 1$.

Due to the severe broadening of the diffraction reflections in the low potential region, it is difficult to obtain a satisfying fit of the XRD patterns below 0.3 V. Nevertheless, the lattice parameters can be accurately determined by the positions of diffraction peaks. The results indicate that the unit cell expansion continues in the low potential region between 0.3 and 0 V (see Table 1). Assuming Vegard's law, the intercalated sodium composition is calculated for the material cycled to 0 V. The resulting sodium composition at 0 V is $Na_{2+2.11}Ti_6O_{13}$, consistent with the upper limit determined by DFT ($Na_{2+2}Ti_6O_{13}$). The comparison between the observed XRD pattern at 0 V and the simulated diffraction patterns using the DFT structures at $x = 2$, 3, 4 in $Na_{2+x}Ti_6O_{13}$, presented in

dx.doi.org/10.1021/ic5004269 | Inorg. Chem. 2014, 53, 8250−8256

Figure S.I.2 in the Supporting Information, indicates best agreement with the $x = 2$ DFT predicted structure. This is consistent with the bulk composition $x = 2.11$ derived from the lattice parameters using Vegard's law, indicating that at 0 V vs Na/Na^+ the bulk composition is close to $x = 2$.

Comparing the $Na_{2+1}Ti_6O_{13}$ and $Na_{2+2}Ti_6O_{13}$ structures in Figures 5b and 5c, Na addition leads to migration of the 2d site toward the adjacent 4i site resulting in minor lattice changes (0.98%), also in good agreement with the XRD results in Table 1 (0.99%).

Upon further sodium insertion (exceeding $Na_{2+2}Ti_6O_{13}$) the BVS value (see Table S.I.1 in the Supporting Information) increases significantly from $Na_{2+2}Ti_6O_{13}$ to $Na_{2+3}Ti_6O_{13}$, implying a lack of space in the 3D tunnel structure for the inserted Na ions making these structures unlikely to form in reality, consistent with DFT that predicts a negative voltage vs Na/Na^+. When the cell is charged to ~0 V, the diffraction peaks irreversibly decrease in intensity and increase in width. This may be a sign of effective loss in particle size and/or crystallinity, potentially responsible for the poor reversibility at low voltages. This may indicate that part of the total capacity at 0 V is due to a reaction of Na at the surface of $Na_2Ti_6O_{13}$. For instance higher Na insertion compositions at the surface may lead to strain or structural disorder, factors that both lead to diffraction line broadening. In addition, the poor reversibility could be the result of side reactions. Several comprehensive studies on structural evolution and electrochemical behavior of Na-inserted hard carbon cycled to 0 V demonstrate the formation of the solid electrode/electrolyte interface (SEI) on the surface of the electrode.[13,33] The continuous growing SEI on the surface of hard carbon, caused by the continuous decomposition of the $NaClO_4$-PC electrolyte upon cycling, is suggested to be the main reason for the capacity fading in carbonaceous materials with $NaClO_4$-PC after 30 cycles.[34] Although the study of SEI formed on transition metal oxide materials is absent to date, we anticipate that electrolyte reduction and decomposition may also take place at the $Na_2Ti_6O_{13}$ surface. Further efforts should be directed toward optimizing the electrolyte as was recently achieved for Na insertion in anatase using $NaPF_6$ in EC:PC.[34]

Also in the similar $Na_2Ti_3O_7$ structure reported recently[21] two-thirds of the Ti^{4+} states are converted to the Ti^{3+} states in the same voltage window (from 2.5 to 0 V) resulting in a similar reversible capacity (~200 mAh/g). In addition, the cycling stability of $Na_2Ti_3O_7$ is excellent when the cutoff voltage is increased from 0.01 to 0.1 V.[35] However, as the sodium 2e sites in $Na_2Ti_3O_7$ have already been fully occupied in the pristine $Na_2Ti_3O_7$ structure, more structural rearrangements are required to accommodate additional sodium in $Na_2Ti_3O_7$ compared to $Na_2Ti_6O_{13}$. Most likely this is the reason why, upon sodium intercalation in $Na_2Ti_3O_7$, new reflections appear at the expense of the original main reflections, indicating a phase transition, while in $Na_2Ti_6O_{13}$ a solid solution mechanism is observed.

CONCLUSIONS

In conclusion, by lowering the cutoff voltage $Na_2Ti_6O_{13}$ to 0 V a promising reversible capacity of nearly 200 mAh/g is found accompanied by minor structural changes following a predominantly solid solution mechanism. This makes $Na_2Ti_6O_{13}$ a promising negative electrode material for Na-ion batteries as compared to other titanium oxide materials such as TiO_2 anatase[19,20,22,32,36] and $Na_4Ti_5O_{12}$.[37] However, the challenge is to extend the reversible capacity over more cycles which may be achieved by electrolytes resulting in a more stable SEI. DFT predicts that the voltage region around 0.8 V vs Na/Na^+ corresponds to the intercalation of the sodium ions at the 2d sites in the tunnel and that only two sodium ions are able to intercalate in the structure of $Na_2Ti_6O_{13}$ above 0 V vs Na/Na^+. Further Na addition is suggested to react at the surface of $Na_2Ti_6O_{13}$ and to be potentially responsible for the observed loss in crystallinity and/or decrease in particle size.

ASSOCIATED CONTENT

Supporting Information

Contribution from carbon, PVDF additives and the residual TiO_2 anatase to total capacity, diffraction patterns based on DFT modeling, full in situ and ex situ XRD patterns, and details of the modeled and fitted structural parameters. This material is available free of charge via the Internet at http://pubs.acs.org.

AUTHOR INFORMATION

Corresponding Author

*E-mail: M.Wagemaker@tudelft.nl.

Notes

The authors declare no competing financial interest.

ACKNOWLEDGMENTS

The Netherlands Organization for Scientific Research (NWO) is acknowledged for the CW-VIDI grant of M.W. The research leading to these results has received funding from the European Research Council under the European Union's Seventh Framework Programme (FP/2007-2013)/ERC Grant Agreement n. [307161] of M.W.

REFERENCES

(1) Whittingham, M. S. *Prog. Solid State Chem.* **1978**, *12*, 44−99.
(2) Nagelberg, A. S.; Worrell, W. L. *J. Solid State Chem.* **1979**, *29*, 345−354.
(3) Molenda, J.; Delmas, C.; Hagenmuller, P. *Solid State Ionics* **1983**, *9&10*, 431−436.
(4) Delmas, C.; Braconnier, J.-J.; Fouassier, C.; Hagenmuller, P. *Solid State Ionics* **1981**, *3*−*4*, 165−169.
(5) Tarascon, J. M.; Hull, G. W. *Solid State Ionics* **1986**, *22*, 85−96.
(6) Abraham, K. M. *Solid State Ionics* **1982**, *7*, 199−212.
(7) Chevrier, V. L.; Ceder, G. *J. Electrochem. Soc.* **2011**, *158*, A1011−A1014.
(8) Palomares, V.; Serras, P.; Villaluenga, I.; Hueso, K. B.; Carretero-Gonz a lez, J.; Rojo, T. O. F. *Energy Environ. Sci.* **2012**, *5*, 5884−5901.
(9) Ong, S. P.; Chevrier, V. L.; Hautier, G.; Jain, A.; Moore, C.; Kim, S.; Ma, X.; Ceder, G. *Energy Environ. Sci.* **2011**, *4*, 3680−3688.
(10) Alcántara, R.; Jiménez-Mateos, J. M.; Lavela, P.; Tirado, J. L. *Electrochem. Commun.* **2001**, *3*, 639−642.
(11) Stevens, D. A.; Dahn, J. R. *J. Electrochem. Soc.* **2000**, *147*, 1271−1273.
(12) Wenzel, S.; Hara, T.; Janek, J. U. R.; Adelhelm, P. *Energy Environ. Sci.* **2011**, *4*, 3342−3345.
(13) Komaba, S.; Murata, W.; Ishikawa, T.; Yabuuchi, N.; Ozeki, T.; Nakayama, T.; Ogata, A.; Gotoh, K.; Fujiwara, K. *Adv. Funct. Mater.* **2011**, *21*, 3859−3867.
(14) Cabana, J.; Monconduit, L.; Larcher, D.; Palacin, M. R. *Adv. Energy Mater.* **2010**, *22*, E170−E192.
(15) Didier, C.; Guignard, M.; Denage, C.; Szajwaj, O.; Ito, S.; Saadoune, I.; Darriet, J.; Delmas, C. *Electrochem. Solid-State Lett.* **2011**, *14*, A75−A78.
(16) Hamani, D.; Ati, M.; Tarascon, J.-M.; Rozier, P. *Electrochem. Commun.* **2011**, *13*, 938−941.

(17) Xiong, H.; Slater, M. D.; Balasubramanian, M.; Johnson, C. S.; Rajh, T. *J. Phys. Chem. Lett.* **2011**, *2*, 2560−2565.
(18) Xu, Y.; Memarzadeh Lotfabad, E.; Wang, H.; Farbod, B.; Xu, Z.; Kohandehghan, A.; Mitlin, D. *Chem. Commun. (Cambridge, U.K.)* **2013**, *49*, 8973−8975.
(19) Wu, L.; Buchholz, D.; Bresser, D.; Gomes Chagas, L.; Passerini, S. *J. Power Sources* **2014**, *251*, 379−385.
(20) Kim, K.-T.; Ali, G.; Chung, K. Y.; Yoon, C. S.; Yashiro, H.; Sun, Y.-K.; Lu, J.; Amine, K.; Myung, S.-T. *Nano Lett.* **2014**, *14*, 416−422.
(21) Senguttuvan, P.; Rousse, G.; Seznec, V.; Tarascon, J.-M.; Palacin, M. R. *Chem. Mater.* **2011**, *23*, 4109−4111.
(22) Rudola, A.; Saravanan, K.; Devaraj, S.; Gong, H.; Balaya, P. *Chem. Commun. (Cambridge, U.K.)* **2013**, *49*, 7451−7453.
(23) Larson, A. C. *GSAS*; Los Alamos National Laboratory: 1994.
(24) Blöchl, P. E. *Phys. Rev. B: Condens. Matter Mater. Phys.* **1994**, *50*, 17953−17979.
(25) Kresse, G.; Furthmüller, J. *Phys. Rev. B: Condens. Matter Mater. Phys.* **1996**, *54*, 11169−11186.
(26) Kresse, G.; Joubert, D. *Phys. Rev. B: Condens. Matter Mater. Phys.* **1999**, *59*, 1758−1775.
(27) Pérez-Flores, J. C.; García-Alvarado, F.; Hoelzel, M.; Sobrados, I.; Sanz, J.; Kuhn, A. *Dalton Trans.* **2012**, *41*, 14633−14642.
(28) Torres-Martínez, L. M.; Juárez-Ramírez, I.; Del Ángel-Sánchez, K.; Garza-Tovar, L.; Cruz-López, A.; Del Ángel, G. *J. Sol-Gel Sci. Technol.* **2008**, *47*, 158−164.
(29) Andersson, S.; Wadsley, A. D. *Acta Crystallogr.* **1962**, *15*, 194−201.
(30) Brown, I. D.; Altermatt, D. *Acta Crystallogr.* **1985**, *41*, 244−247.
(31) Adams, S. *Acta Crystallogr., Sect. B: Struct. Sci.* **2001**, *57*, 278−287.
(32) Zhou, F.; Cococcioni, M.; Kang, K.; Ceder, G. *Electrochem. Commun.* **2004**, *6*, 1144−1148.
(33) Gotoh, K.; Ishikawa, T.; Shimadzu, S.; Yabuuchi, N.; Komaba, S.; Takeda, K.; Goto, A.; Deguchi, K.; Ohki, S.; Hashi, K.; Shimizu, T.; Ishida, H. *J. Power Sources* **2013**, *225*, 137−140.
(34) Ponrouch, A.; Marchante, E.; Courty, M.; Tarascon, J.-M.; Palacin, M. R. *Energy Environ. Sci.* **2012**, *5*, 8572−8583.
(35) Rudola, A.; Saravanan, K.; Mason, C. W.; Balaya, P. *J. Mater. Chem. A* **2013**, *1*, 2653−2662.
(36) Lindström, H.; Södergren, S.; Solbrand, A.; Rensmo, H.; Hjelm, J.; Hagfeldt, A.; Lindquist, S.-E. *J. Phys. Chem. B* **1997**, *101*, 7710−7716.
(37) Woo, S. H.; Park, Y.; Choi, W. Y.; Choi, N. S.; Nam, S.; Park, B.; Lee, K. T. *J. Electrochem. Soc.* **2012**, *159*, A2016−A2023.